Experimental measurements and correlation of vapor-liquid equilibrium data for the difluoromethane (R32) + 1,3,3,3-tetrafluoropropene (R1234ze(E)) binary system from 254 to 348 K

Pierre Six, Alain Valtz, Yulong Zhou, Zhiqiang Yang, Christophe Coquelet

Experimental measurements and correlation of vapor-liquid equilibrium data for the difluoromethane (R32) + 1,3,3,3-tetrafluoropropene (R1234ze(E)) binary system from 254 to 348 K

Pierre Six[1], Alain Valtz[1], Yulong Zhou[2], Zhiqiang Yang[2,3*], Christophe Coquelet[1,4*]

1 Mines Paris PSL University, CTP-Centre of Thermodynamics of Processes, 35 Rue Saint Honoré, 77305 Fontainebleau, France.

2 Key Laboratory of Thermo-Fluid Science and Engineering, Ministry of Education, Xi'an Jiaotong University, Xi'an, 710049, China

3 State Key Laboratory of Fluorine & Nitrogen Chemicals, Xi'an Modern Chemistry Research Institute, Xi'an, 710065, China

4 Université de Toulouse, IMT Mines Albi, CNRS UMR 5302, Centre Rapsodee Campus Jarlard, 81013 Albi CT Cedex 9, France.

In this study, we present new experimental data of vapor-liquid equilibrium for the binary system difluoromethane (R32) + 1,3,3,3-tetrafluoropropene (R1234ze(E)), measured at 273.14 and 363.32 K and at pressure ranging from 0.1568 to 4.3553 MPa. A "static-analytic"-type apparatus is used to do the measurements, with sampling of the equilibrium phases via capillary sampler (ROLSI®). We used three different models to correlate the data: 1) the Peng-Robinson cubic equation of state combined with the NRTL excess free energy model and Wong-Sandler mixing rules, 2) Helmholtz energy model like the one incorporated in REFPROP 10.0 software and 3) Predictive PPR78 model for which the new group parameter of R32 was adjusted. All of the three models show a very good agreement with the experimental data except for temperature higher that R32 critical temperature.

Keywords: VLE data, R32, R1234ze(E), critical point, EoS.

* Corresponding authors: Christophe.coquelet@mines-albi.fr; zqyang@stu.xjtu.edu.cn

1. Introduction

Hydrofluorocarbons (HFCs) are potent greenhouse gases developed as replacements for ozone-depleting substances, and have long been widely used as refrigerants in vapor compression-based refrigeration, air-conditioning, and heat pump [1]. Since greenhouse gases are the most important driver of climate change, environmental impacts become the main indicator of current refrigerants, which poses the biggest constraint on the utilization of existing HFCs. A phase-down of HFCs was mandated in the European Union in 2016 and a global phase-down is in negotiation [2]. Researchers and developers are forced to find candidates for refrigerants with low global warming potential (GWP), short atmospheric lifetime, and high efficiency [3].

Recently, a highly promising alternative solution for refrigeration and heat pump systems has been proposed in the form of a next-generation refrigerant called *trans* -2,2,3,3-tetrafluoropropo-1-ene (R1234ze(E)). R1234ze(E) shows a combination of zero ozone-depletion potential, low GWP, low toxicity and excellent chemical and thermophysical properties necessary for a work fluids [4]. One of disadvantage of R1234ze(E) is the flammability. It is categorized as class A2L according to ASHRAE. Additionally, compared to R134a, R1234ze(E) has a lower latent heat of vaporization, resulting in larger mass flow rates and pressure drops in heat exchangers and connection pipes. Consequently, this leads to lower coefficients of performance [5] .

To assess the performance of R1234ze(E) in practical applications, it is essential to measure its thermophysical properties, especially its thermodynamic properties. Since R1234ze(E) is often considered as a component in refrigerant blends, understanding the thermodynamic properties of binary systems involving R1234ze(E) is crucial. Knowledge

of the vapor-liquid equilibrium of these blends is vital for evaluating temperature and pressure glide for a given overall composition, assessing system performance using parametrized mixture equations of state, and examining performance modifications in the event of leakage. In the case of heat exchangers utilizing a working fluid and aqueous glycol solution, employing a working fluid with temperature glide is preferable to achieve improved performance.

In the literature it exists several studies involving the R1234ze(E) and other chemicals. From our research team, we can cite the works from Liu et al. [6] with R160 (ethane), Yang et al. [7] with R1243zf, Wang et al. [8] with R744 (CO_2) [8]. R32 is one of the commercial HFC with the GWP less than 600 [9]. It is also well used for heat pump and refrigeration applications. The current paper presents new vapor-liquid equilibrium (VLE) data for the R32 + R1234ze(E) binary system at seven temperatures (273.14, 293.17, 313.20, 333.27, 353.53 and 363.32 K). Like R1234ze(E), R32 is categorized according to ASHRAE as class A2L weakly flammable. Consequently, the mixture of R32 + R1234ze(E) will be also classified as A2L concerning the risk of flammability. Four isotherms are below the critical temperature of R32 and two are above it. This binary system was previously studied by Hu et al. [10]. They have determined VLE data in the whole range of composition at 5 temperatures from 283.15 to 323.15 K. In 2013, Akasaka [11] has published an explicit Helmholtz energy model, used in REFPROP 10.0 [12] concerning R32+R1234ze(E) binary systems. It is mentioned in this paper that data from paper presented at several Japan congresses and molecular simulation data were considered (for VLE and critical point properties). We also proposed in this work to compare our data and data from Hu et al. [10] to REFPROP calculations.

Two different thermodynamic methods are used to model the system. The first one is based on the Peng-Robinson (PR) cubic equation of state (EoS) [13] using the original alpha function, combined with the the Wong-Sandler (WS) mixing rules [14] involving the Non-Random Two Liquids (NRTL) activity coefficient model [15] (PR WS NRTL). The second model is based on the predictive Peng Robinson Eos (PPR78 [16]).

2. Experimental Section

2.1 Materials

All pure compounds were obtained commercially and used without any additional purification. The purities and the suppliers of the compounds are listed in Table 1.

Table 1: Purity and supplier of the chemical compounds used in this work.

Compound	CAS number	Purity /wt%	Supplier	Analysis method	Critical properties from REFPROP V10.0 [12] [12]	
					T_c/K	P_c/MPa
R1234ze(E)	29118-24-9	99.5 wt%	Climalife	GC	382.51	3.635
R32	75-10-5	99.5 wt.%	Climalife	GC	351.26	5.782

GC: Gas Chromatography

2.2 Apparatus

The apparatus used in this work is based on a “static-analytic” method with liquid and vapor phase sampling (Coquelet et al. [17]). This apparatus is similar to the equipment used in previous studies, details can be found from Wang et al. [8] and described by Afzal et al. [18]. The apparatus is equipped with two online capillary samplers (Armines’s patent [19]) which are capable of withdrawing and sending micro samples, through

heated transfer line to avoid sample condensation, to a gas chromatograph without perturbing the equilibrium conditions over numerous samplings, thus leading to repeatable and reliable results. The equilibrium cell comprises of a sapphire tube that is held in place by two Hastelloy flanges equipped with suitable O-rings. Each flange incorporates valves for loading and cleaning the cell. A vertical magnetic stirrer, capable of handling multiple phases, is positioned at the centre of the sapphire tube to ensure thorough mixing. To protect the stirring assembly from the corrosive environment, it is covered with a corrosion-resistant shield. The agitation mechanism is magnetically coupled to an external motor, which provides the desired level of agitation within the cell. For temperature measurement, two calibrated 100 Ω platinum resistance thermometer sensors (Pt-100) are utilized. These sensors are placed at the lower and upper sections of the cell to enable the examination and prevention of temperature gradients. To measure equilibrium pressures, two calibrated Druck pressure transducers (PTX 611) are employed—one for the lower pressure range [0-2 MPa] and the other for the higher-pressure range [0-7 MPa]. Both pressure transducers are kept at a constant temperature (higher than the maximum temperature of the study) and their temperature is regulated using a PID controller (WEST instrument, model 6100). You can refer to Figure 1 for a schematic diagram of the experimental setup.

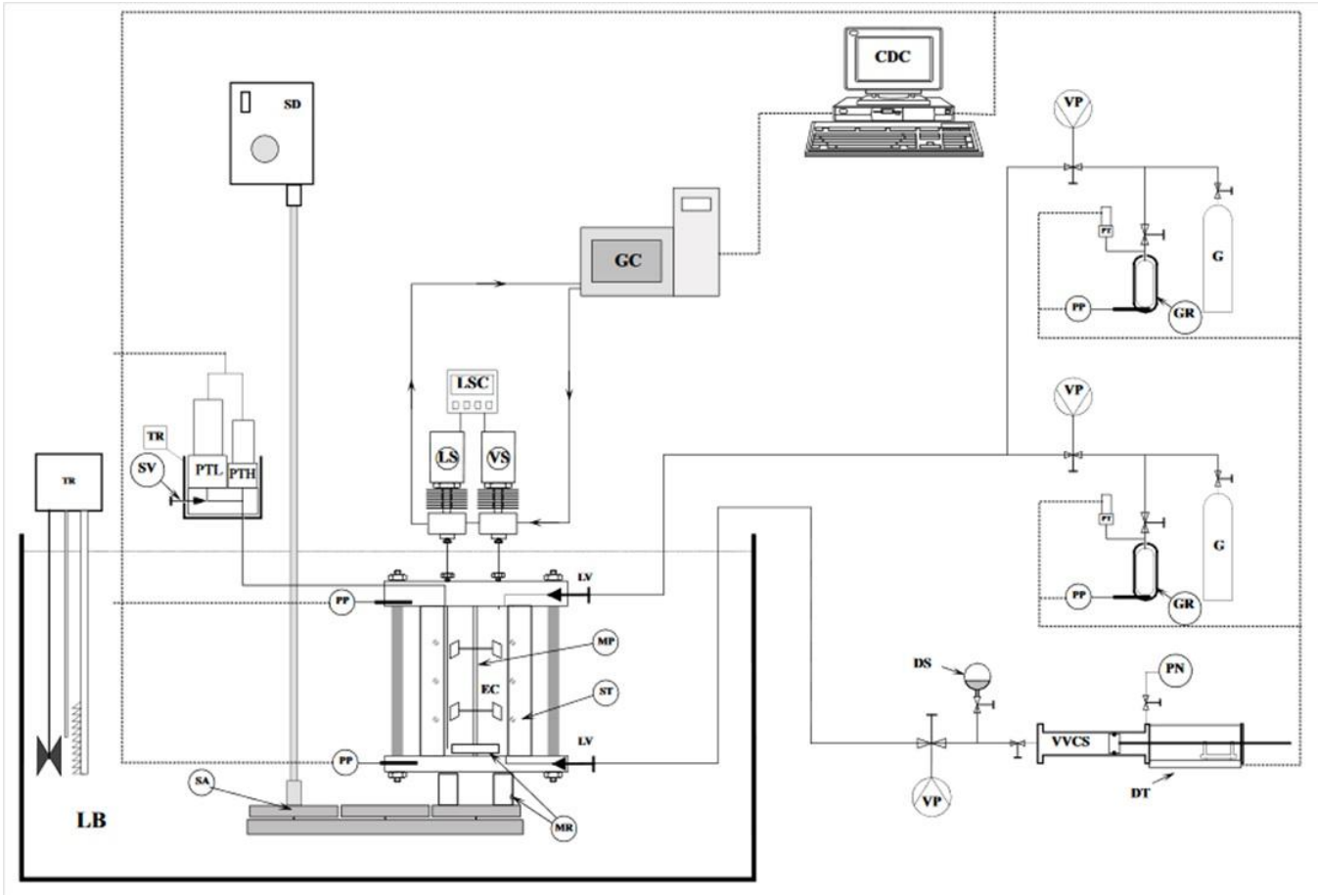

Figure 1: Flow diagram of the high-pressure apparatus. CDC: Central desktop computer, DS: Degassed solution, DT: Displacement transducer, EC: Equilibrium cell, G: Gas cylinder, GC: Gas chromatograph, GR: Gas reserve, LB: Liquid bath, LS: Liquid sampler, LSC: Local sample controller, LV: Loading valve, MR: Magnetic rod, MP: Multiple phase agitator, PN: Pressurized nitrogen, PP: Pt temperature sensor, PT: Pressure transducer (L: Low pressure and H: High pressure), SA: Stirring assembly, SD: Stirring device (motor), ST: Sapphire tube, SV: Separation valve, TR: Temperature controller, VP: Vacuum pump, VS: Vapor sampler, VVCS: Variable volume cell.

The Pt100 probes are calibrated against a 25 Ω reference probe (TINSLEY Precision Instrument) certified by the Laboratoire National d'Essais (Paris) following the International Temperature Scale 1990 protocol. Pressure transducer are calibrated against a dead weight pressure balance (5202S model from Desgranges & Huot).

Temperature and pressure data acquisition is performed with a computer linked to an HP unit (HP34970A). The resulting uncertainties in this work are u(T, k=2)=0.02 K for the two platinum probes and u(P, k=2)=0.0005 MPa for the two pressure transducers.

The analytical work was carried out using a gas chromatograph equipped with a thermal conductivity detector (TCD) connected to a data acquisition system.

The analytical column used for the separation was a 1% RT 1000 on CarboBlack B model with 60/80 mesh (2 mm internal diameter, Silcostell tube, 2.4 m length) from RESTEK. The TCD was calibrated multiple times by introducing known quantities of each pure compound through a syringe into the gas chromatograph's injector. The resulting relative accuracies in mole numbers are ±0.9% for R32 and ±1.3% for R1234ze(E).

The uncertainty on mole fraction due to the calibration of the GC detector can be calculated as a function of the relative uncertainty on each mole number by Eq. (1).

$$u_{cal}(x_1) = x_1(1 - x_1)\sqrt{\sum_1^2 \left(\frac{u_r(n_i)}{\sqrt{3}}\right)^2} \quad (1)$$

2.3 Experimental Procedure

At room temperature, the equilibrium cell and its loading lines are evacuated to a pressure of 0.1 Pa. The cell is initially filled with a liquid form of R1234ze(E) in a quantity of less than 5 cm3. Equilibrium temperature is considered to be reached when

the two Pt100 probes (one located at the top of the equilibrium cell and the other at the bottom) provide temperature readings that are within the experimental uncertainty and remain equivalent for at least 10 minutes. The vapor pressure of R1234ze(E) (the heavier component) is then measured at the equilibrium temperature. Subsequently, R32 (the lighter component) is introduced gradually, resulting in a series of equilibrium mixtures with increasing overall R32 content. After each addition of R32, equilibrium is assumed to be reached when the total pressure remains stable within ±1.0 kPa for a period of 10 minutes, with efficient stirring.

For each equilibrium condition, at least five samples of both vapor and liquid phases are extracted using ROLSI® capillary samplers [19] and analysed to verify the repeatability of the measurements.

3. Thermodynamic modeling

The system was modeled by means of an in-house software. For the pure compounds, we used the PR EoS [13] with the original alpha function. The critical temperatures (T_C) and critical pressures (P_C) for each of the two pure components are provided in Table 1. We applied the PR EoS to the mixture by using the Wong-Sandler mixing rules for both vapor and liquid phases, defined by [14] (Eqs. 2 – 4).

$$b = \frac{\sum_i \sum_j z_i z_j \left(b_{ij} - \frac{a_{ij}}{RT} \right)}{1 - \left(\frac{\sum_i z_i \frac{a_i}{b_i}}{RT} + \frac{g^E\left(T, P = \infty, z_i\right)}{CRT} \right)} \quad (2)$$

and

$$b - \frac{a}{RT} = \sum_i \sum_j z_i z_j \left(b_{ij} - \frac{a_{ij}}{RT} \right) \tag{3}$$

with

$$b_{ij} - \frac{a_{ij}}{RT} = \frac{1}{2} \left[\left(b_i - \frac{a_i}{RT} \right) + \left(b_j - \frac{a_j}{RT} \right) \right] \left(1 - k_{ij}\right) \tag{4}$$

z_i is the mole fraction (vapor or liquid). k_{ij} is an adjustable binary interaction parameter and C is a constant equal to 0.62323. The model chosen for the excess Gibbs energy (g^E) is the NRTL [15] local composition model (Eq. 5).

$$\frac{g^E(T, P, z_i)}{RT} = \sum_i z_i \sum_j \frac{z_j \exp\left(-\alpha_{ji}\tau_{ji}\right)}{\sum_k z_k \exp\left(-\alpha_{ki}\tau_{ki}\right)} \tau_{ji} \tag{5}$$

where α_{ij} and τ_{ij} are the adjustable parameters of the NRTL model, with $\tau_{ii} = 0$ and $\alpha_{ii} = 0$.. It is recommended to use a value of α_{ij} ($=\alpha_{ji}$) equal to 0.3 for systems involving a polar compound [15]. τ_{12} and τ_{21} are adjusted directly to VLE data through a modified simplex algorithm [19], using the following objective function (flash algorithm, Eq. 6):

$$F = \frac{100}{N} \left[\sum_1^N \left(\frac{x_{\exp} - x_{cal}}{x_{\exp}} \right)^2 + \sum_1^N \left(\frac{y_{\exp} - y_{cal}}{y_{\exp}} \right)^2 \right] \tag{6}$$

where N is the number of data points, x_{exp} and x_{cal} the measured and calculated liquid phase mole fractions, and y_{exp} and y_{cal} the measured and calculated vapor phase mole fractions, respectively.

In order to analyze the results, we will use two indicators. The average absolute deviation, AAD, and the BIAS applied on vapor pressure and, liquid and vapor phase mole fractions, are defined by Eqs 7 and 8.

$$AAD = (100 / N)\sum \left|(U_{cal} - U_{exp})/U_{exp}\right| \quad (7)$$

$$BIAS = (100 / N)\sum \left((U_{exp} - U_{cal})/U_{exp}\right) \quad (8)$$

where N is the number of data points, and U is p, x_1 or y_1.

4. Results and discussion:

4.1 Vapor pressures data

We have measured vapor pressures for the pure component of R1234ze(E) and the experimental results are compared with calculations from REFPROP 10.0 [12] (Table 2). We observed that relative deviations between experimental data and REFPROP calculations are lower than 1% (with REFPROP AAD (Average Absolute Deviation) =0.2% with Bias=0.1%; with PR EoS AAD=0.9% with bias=0.3%). REFPROP claims that the uncertainty in vapor pressure is 0.1%.

Table 2: Comparison between experimental R1234ze(E) vapor pressure and calculations using REFPROP 10.0 and Peng Robinson EoS. U(*T*) = 0.02 K, U(*P*) = 0.0005 MPa

T /K	P_{exp}/MPa	Calculated pressure /MPa		ΔP/P /%	
		REFPROP 10.0	PR EoS	REFPROP 10.0	PR EoS
273.14	0.2169	0.2165	0.2125	0.20	2.01
293.17	0.4281	0.4276	0.4226	0.11	1.28
313.20	0.7670	0.7675	0.7641	-0.06	0.38
333.27	1.2770	1.2802	1.2838	-0.25	-0.53
353.53	2.0294	2.0241	2.0424	0.26	-0.64
363.32	2.4971	2.4842	2.5112	0.52	-0.57

We have also compared R32 vapor pressures calculated using Peng Robinson EoS with one calculated using REFPROP 10.0. No R32 vapor pressure data was measured. Considering the indicators, we have an AAD=0.7% and a Bias=-0.7%. The classical alpha function was utilized because some VLE data were measured for temperature higher than the critical temperature of R32 and to have continuity of the alpha function at the R32 critical temperature. In summary, the experimental relative uncertainty is around 0.2%, we can consider good agreement between our experimental data and REFPROP calculation.

4.2 Vapor-liquid equilibrium data for the R32 + R1234ze(E) mixture

The experimental and calculated VLE data are reported in Table 3 and plotted on Figure 3. Figure 4 presents the experimental and calculated relative volatility as a function of mole fraction. We can observe the good exponentially declined trend of relative volatility which valid the correctness of VLE measurements. The adjusted parameters are given in Table 4. The trends of these temperature-dependent binary parameters are plotted in Figures 4 to 6. Taking into account the evolution of the different Binary Interaction Parameters (BIP; τ_{12}, τ_{21} *and* k_{12}) with the temperature. We have also adjusted the BIP using data where temperature is higher than the critical temperature of

R32 with no temperature dependency (see Table 4). We can observed that BIP behavior differs in the subcritical and supercritical region relative to the critical temperature of pure R32. AAD and Bias indicators, which give information about the agreement between model and experimental results, are presented in Table 5.

Table 3: Experimental isothermal VLE data for the R32 (1) + R1234ze(E) (2) mixture system and their standard uncertainties U(T) = 0.02 K, U(P) = 0.0005 MPa, $U_{cal}(x, y)$= <0.013.

	Experimental data				*Calculated with* PR-WS-NRTL *Model*	
P/MPa	x_1	$u_{rep}(x_1)$	y_1	$u_{rep}(y_1)$	x_1	y_1
			T=273.14 K			
0.2169	0.0000		0.0000			
0.3039	0.1206	0.0002	0.3445	0.0015	0.1209	0.3528
0.4067	0.2741	0.0004	0.5684	0.0014	0.2734	0.5770
0.4067	0.2743	0.0011	0.5736	0.0016	0.2734	0.5770
0.5019	0.4283	0.0043	0.7075	0.0023	0.4274	0.7109
0.5986	0.5965	0.0011	0.8236	0.0003	0.5961	0.8132
0.6070	0.6078	0.0021	0.8250	0.0010	0.6112	0.8212
0.7041	0.7815	0.0007	0.9074	0.0009	0.7901	0.9070
			T=293.17 K			
0.4281	0.0000		0.0000			
0.5234	0.0809	0.0065	0.2198	0.0004	0.0777	0.2270
0.6556	0.1933	0.0007	0.4235	0.0011	0.1920	0.4376
0.7600	0.2851	0.0079	0.5442	0.0020	0.2866	0.5576
0.8863	0.4059	0.0031	0.6692	0.0012	0.4043	0.6699
1.0334	0.5463	0.0025	0.7719	0.0001	0.5452	0.7717
1.1538	0.6642	0.0018	0.8413	0.0001	0.6640	0.8404
1.2994	0.8118	0.0011	0.9118	0.0007	0.8115	0.9131
1.3831	0.8949	0.0003	0.9524	0.0000	0.8968	0.9523
			T=313.20 K			
0.7670	0.0000		0.0000			
0.9360	0.0895	0.0001	0.2180	0.0006	0.0888	0.2199
1.1922	0.2328	0.0001	0.4509	0.0008	0.2342	0.4499
1.4429	0.3791	0.0003	0.6070	0.0020	0.3810	0.6076
1.6976	0.5305	0.0001	0.7299	0.0006	0.5307	0.7290
1.9457	0.6766	0.0005	0.8242	0.0001	0.6766	0.8242
2.2517	0.8588	0.0002	0.9260	0.0017	0.8557	0.9239
			T=333.27 K			
1.2770	0.0000		0.0000			

3.5399	0.8550	0.0003	0.8987	0.0025	0.8525	0.9072
1.6375	0.1310	0.0002	0.2615	0.0008	0.1314	0.2602
2.0136	0.2748	0.0001	0.4590	0.0006	0.2797	0.4552
2.3974	0.4248	0.0001	0.6085	0.0007	0.4306	0.6047
2.7782	0.5737	0.0006	0.7248	0.0009	0.5762	0.7224
3.1676	0.7213	0.0002	0.8229	0.0004	0.7202	0.8227
3.5489	0.8590	0.0001	0.9089	0.0006	0.8557	0.9092
			T=353.53 K			
2.0294	0.0000		0.0000			
2.5048	0.1306	0.0001	0.2222	0.0006	0.1322	0.2209
2.9991	0.2656	0.0002	0.3929	0.0004	0.2693	0.3942
3.5056	0.4047	0.0001	0.5329	0.0007	0.4048	0.5321
4.0027	0.5330	0.0004	0.6426	0.0006	0.5327	0.6420
4.4905	0.6578	0.0003	0.7363	0.0005	0.6540	0.7344
4.7492	0.7213	0.0003	0.7818	0.0006	0.7165	0.7794
4.9071	0.7575	0.0003	0.8088	0.0005	0.7540	0.8060
5.0075	0.7792	0.0004	0.8237	0.0007	0.7776	0.8227
5.0954	0.7988	0.0002	0.8382	0.0003	0.7980	0.8372
5.1907	0.8200	0.0005	0.8524	0.0003	0.8199	0.8528
5.2999	0.8440	0.0004	0.8699	0.0003	0.8447	0.8707
5.4067	0.8667	0.0001	0.8859	0.0003	0.8686	0.8882
5.5010	0.8867	0.0004	0.9010	0.0002	0.8894	0.9037
5.6044	0.9125	0.0006	0.9183	0.0008	0.9118	0.9208
			T=363.32 K			
2.4971	0.0000		0.0000			
3.0255	0.1264	0.0002	0.1968	0.0008	0.1316	0.1981
3.4520	0.2310	0.0002	0.3261	0.0019	0.2345	0.3226
3.9293	0.3438	0.0001	0.4422	0.0009	0.3461	0.4366
4.2557	0.4190	0.0001	0.5081	0.0010	0.4205	0.5032
4.4814	0.4700	0.0002	0.5495	0.0008	0.4712	0.5451
4.6966	0.5179	0.0001	0.5862	0.0007	0.5192	0.5823
4.8097	0.5451	0.0003	0.6053	0.0012	0.5443	0.6009
4.9109	0.5676	0.0003	0.6198	0.0009	0.5667	0.6169
5.0275	0.5923	0.0005	0.6345	0.0004	0.5926	0.6347
5.1140	0.6128	0.0002	0.6446	0.0006	0.6120	0.6473
5.1415	0.6229	0.0002	0.6464	0.0008	0.6183	0.6512
5.1659	0.6325	0.0003	0.6372	0.0003	0.6238	0.6546

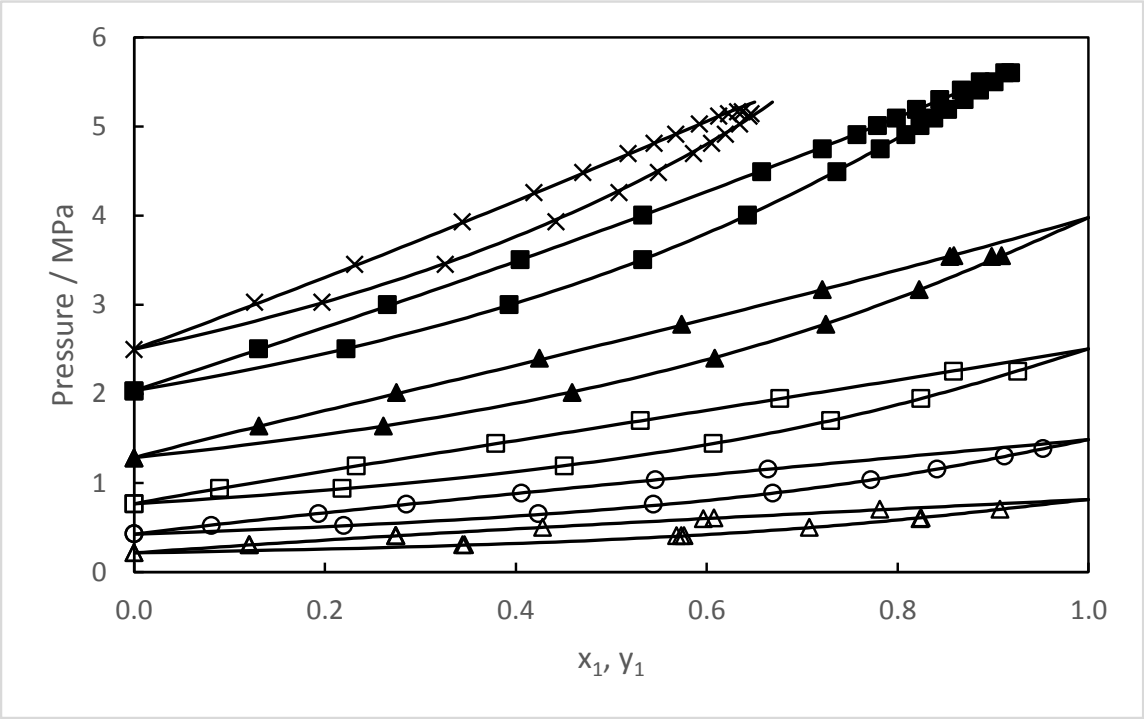

Figure 2. P-x-y diagram of the R32 (1) - R1234ze(E) (2) system. Experimental data: (Δ) 273.14 K; (○) 293.17 K; (□) 313.20 K ; (▲) 333.27 K;(■): 353.53 K; (×) 363.32 K. Modeling: (—) PR-WS-NRTL model.

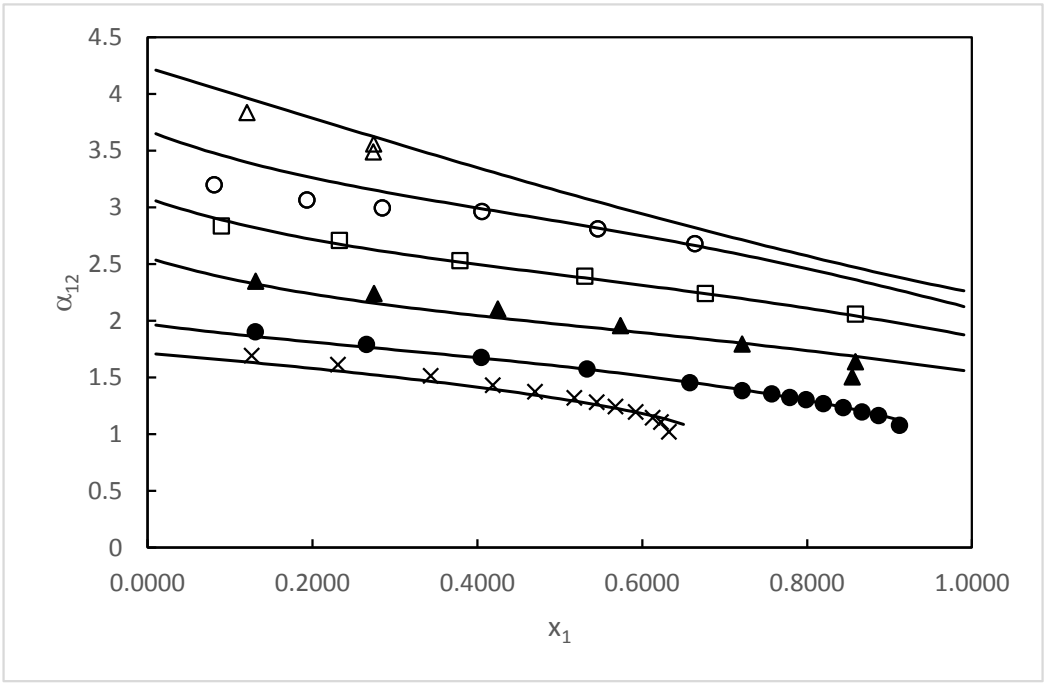

Figure 3. Relative volatility α_{12} for the binary system the CO_2 (1) + R-1234ze(E) (2) mixture at different temperatures. : (Δ) 273.14 K; (○) 293.17 K ; (□) 313.20 K ; (▲) 333.27 K;(■): 353.53 K; (×) 363.32 K. Solid lines: PR-WS-NRTL model.

Table 4: Values of the binary parameters at each temperature for the PR-WS-NRTL model.

T /K	τ_{12}	τ_{21}	k_{12}
273.14	4788	-118	-0.2105
293.17	-2033	3186	0.1856
313.20	-2184	3517	0.1653
333.27	-2298	3807	0.1486
353.53	-2608	3771	0.1817
363.32	-146	470	0.1729
$T>TC_{R32}$	-43	304	0.1703

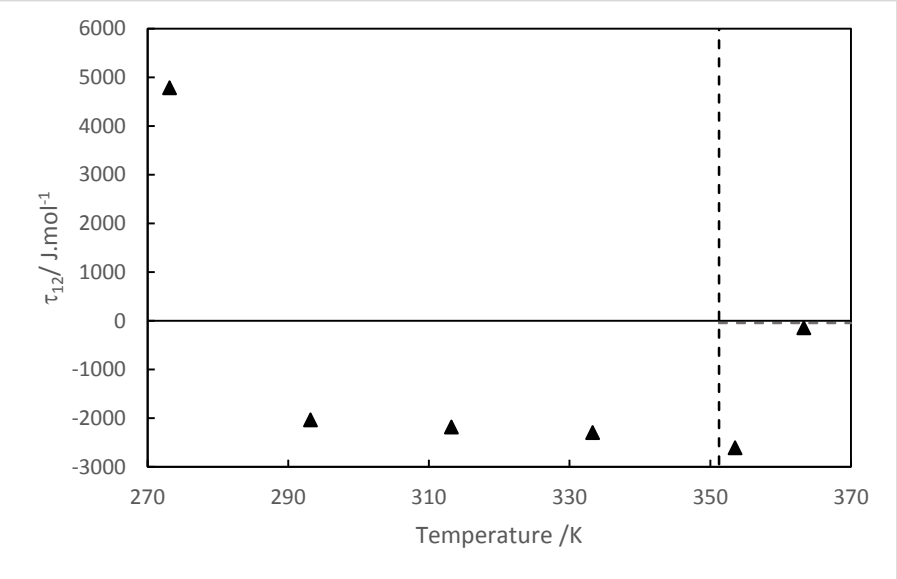

Figure 4: τ_{12} binary parameter as a function of temperature. Vertical dashed: R32 critical temperature. Horizontal dashed line: parameter value obtained after considering all the data for $T > T_c$(R32).

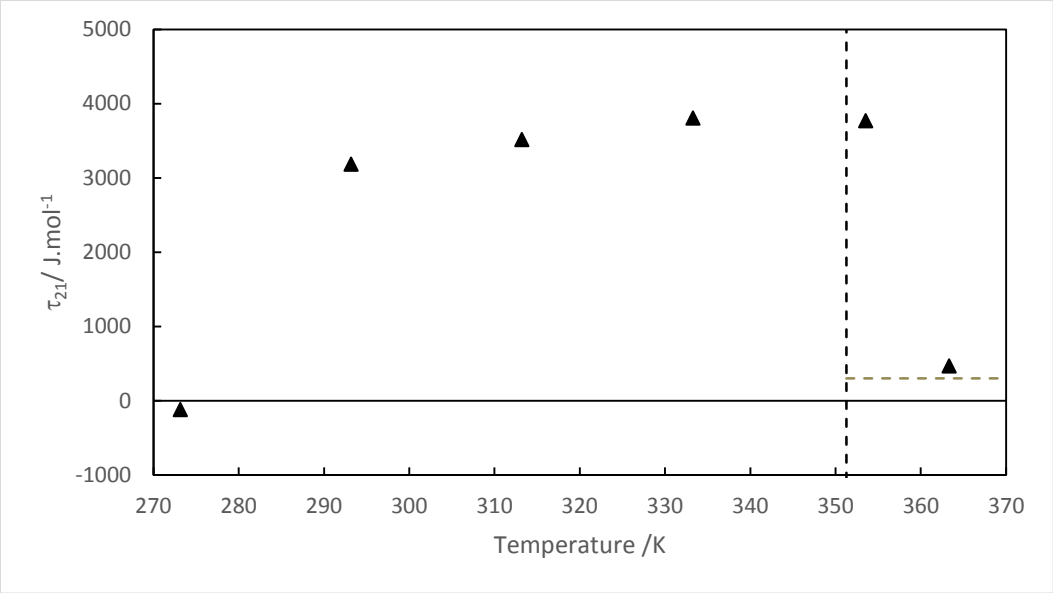

Figure 5: τ_{21} binary parameter as a function of temperature. Vertical dashed: R32 critical temperature. Horizontal dashed line: parameter value obtained after considering all the data for $T > T_c$(R32).

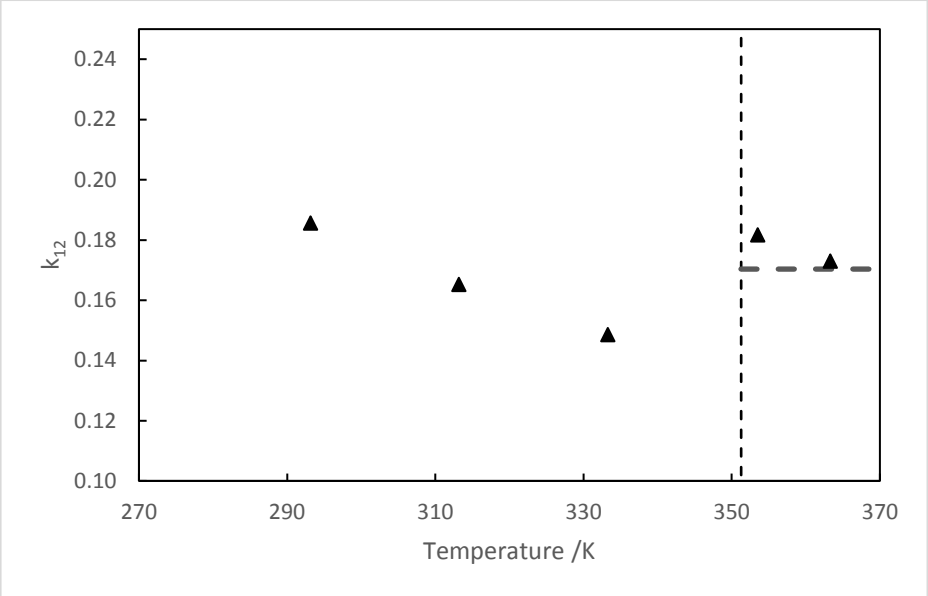

Figure 6: k_{12} binary parameter as a function of temperature. Vertical dashed line: R32 critical temperature. Horizontal dashed line: parameter value obtained after considering all the data for $T > T_c$(R32).

Table 5: AAD and Bias on vapor and liquid mole fractions obtained in fitting experimental VLE data with PR-WS-NRTL model.

***T*/K**	***bias x /%***	***bias y/%***	***AAD x/%***	***AAD y/%***
273.14	-0.15	-0.46	0.40	0.97
293.17	0.57	-1.14	0.76	1.18
313.20	-0.004	-0.06	0.38	0.26
333.27	-0.44	0.19	0.68	0.47
353.53	-0.07	0.05	0.38	0.23
363.32	-0.39	0.12	0.82	0.88
***T*>*T*$_C$ R32**	-0.59	0.02	0.94	0.49

As Akasaka [11] has defined a REFPROP type model for the R32 + R1234ze(E) binary system, we have compared our experimental data with the REFPROP prediction. We have considered a bubble point pressure calculation. In parallel, we have also compared REFPROP calculations to the data publish by Hu et al. [10] for temperature lower than the R32 critical temperature. AAD and Bias indicators, which give information about the agreement between model and experimental results, are presented in Table 6. Both the bias and AAD for p and y are in the same level of deviation, which means the experimental data of this work are in good agreement with Hu et al. [10]. Following theses comparisons, we can conclude that the new experimental data measured in this work are consistent.

Table 6: AAD and Bias on bubble pressure and liquid mole fractions: comparison between REFPROP calculations with Hu et al. literature data and this work.

References	***T*/K**	**Bias *P*/%**	**AAD *P*/%**	**AAD *y*/%**	**Bias *y*/%**
This Work	273.14	-2.78	2.83	-2.85	3.41
	293.17	-1.65	1.76	-1.73	2.92
	313.20	-0.87	0.91	-0.17	1.24
	333.27	-0.23	0.28	0.15	0.68
	353.53	0.39	0.39	-0.20	0.24
	363.32	0.58	0.63	-2.02	2.04
Hu et al.	283.15	-2.24	2.26	-2.01	2.99
	293.15	-1.86	1.86	-1.37	1.80

	303.15	-1.39	1.41	-1.29	1.61
	313.15	-1.12	1.14	-1.58	1.73
	323.15	-0.82	0.83	-2.04	2.04

4.3 Critical lines computation

The isothermal experimental data have been used to estimate the critical point (composition and pressure). The critical loci for binary mixtures and the near-critical behavior were approximated by the use of extended scaling laws, as described previously by Ungerer et al. [21-22] and used in previous work [8]. In this method, the near-critical part of the pressure-composition diagram was represented by complementing the near-critical scaling law with a linear term (Eq. 9).

$$y - x = \lambda_1(P_C - p) + \mu(P_C - P)^{\beta} \quad (9)$$

And Eq. 10 is used for the mid-composition:

$$\frac{y+x}{2} - x_C = \lambda_2(P_C - P) \quad (10)$$

Parameters λ_1, λ_2, μ, P_c and x_c are adjusted using experimental data close to the mixture critical point. The values are reported in Table 7 and plotted on Figure 7.

Table 7: Extended scaling-law parameters λ_1, λ_2, and μ adjusted on experimental data and calculated critical temperature and composition.

T /K	$\lambda_1 * 10^4$	$\lambda_2 * 10^4$	$\mu * 10^3$	x_C	P_C / MPa
353.53	197.82	-1999.68	26.43	0.917	5.613
363.32	199.56	-1999.86	76.81	0.637	5.166

To calculate the critical line using the PR EoS with WS mixing rules involving the NRTL model, we used the method of Stockfleth and Dohrn [22], who proposed a generalized algorithm to calculate the critical points by using any type of EoS and mixing-rule considering Heidemann and Khalil [23, 24] algorithm. The temperature independent binary parameters are those obtained by fitting VLE data in the R32 supercritical domain.

Results are plotted on Figure 7. We have obtained a predicted critical locus line in good agreement with the isothermal phase envelopes.

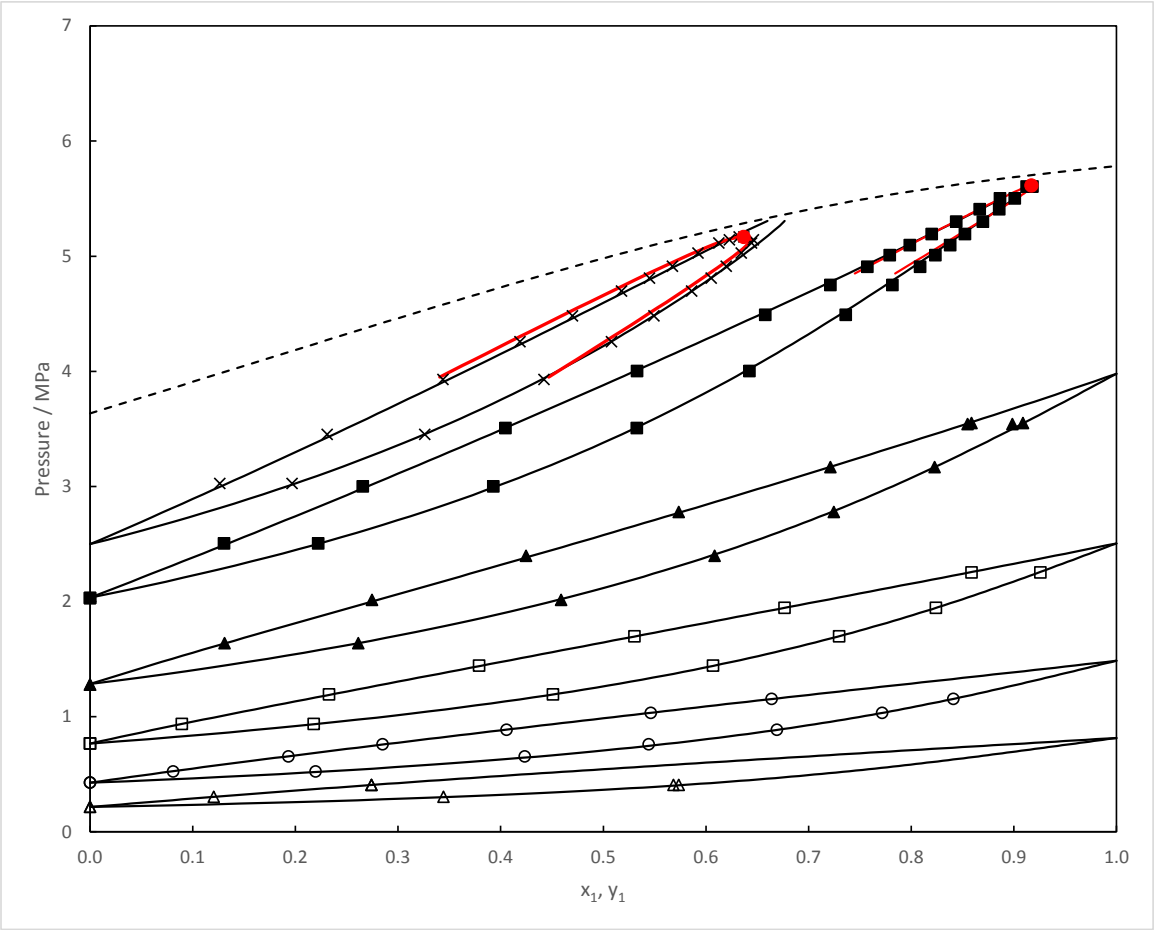

Figure 7: P-x-y diagram of the R32 (1) - R1234ze(E) (2) system.
Experimental data: (Δ) 273.14 K; (○) 293.17 K ; (□) 313.20 K ; (▲) 333.27 K; (■): 353.53 K; (×) 363.32 K Modeling: (—) Peng Robinson EoS
---: mixture critical point line with PR-WS-NRTL model and Heidemann Khalil computational method.
•: Mixture critical point calculated with the asymptotic law behaviour equation (above the critical temperature of R32). Solid red line: calculated using asymptotic law behaviour equation.

On Figure 7, we can see some deviations between pseudo experimental critical point values and the calculated ones by the model. We have also plotted the REFPROP 10.0 prediction for the two last isotherms (Figure 8). As we can see, there is some deviations between PR EoS and REFPROP 10.0 calculations. New experimental data, particularly

the isotherms for temperature above R32 critical temperature have to be taken into account.

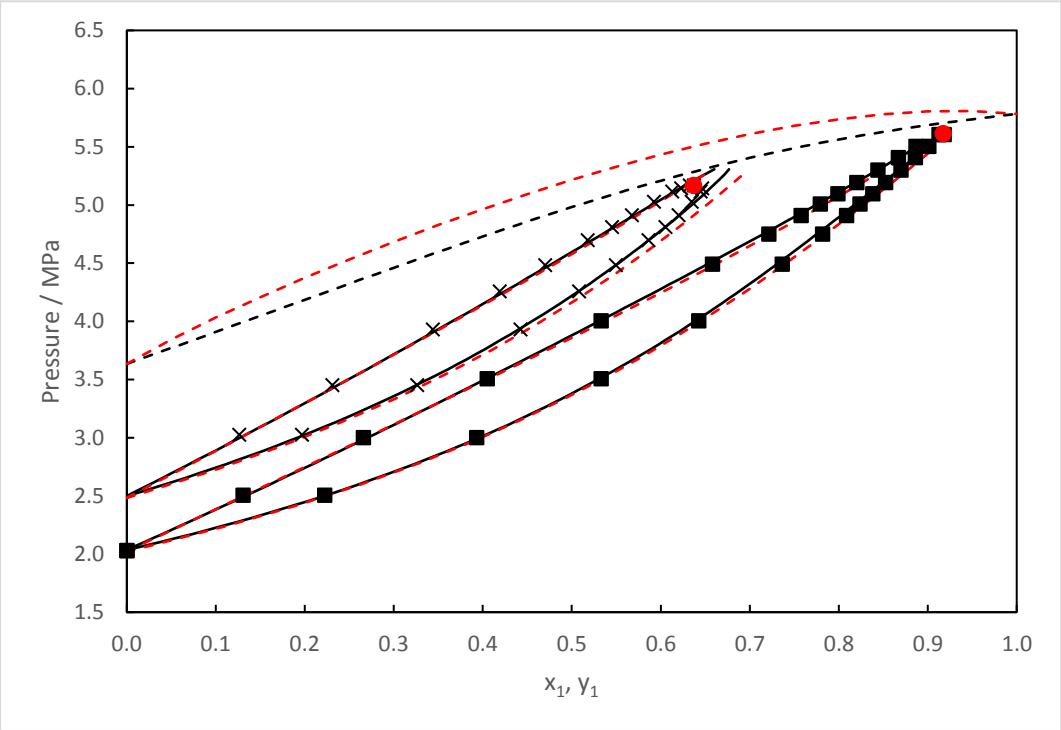

Figure 8: P-x-y diagram of the R32 (1) - R1234ze(E) (2) system.
Experimental data: (■): 353.53 K; (×) 363.32 K. Modeling: solid line: PR-WS-NRTL model, Dashed line: mixture critical point line with Heidemann Khalil computational method.
and red dashed line: calculated using REFPROP 10.0. ●: Mixture critical point calculated with the asymptotic law behaviour (above the critical temperature of R32).

5. PPR78 predictive model

The PPR78 model, a group-contribution (GC) concept model developed by Jaubert et al. [16, 25-26], provides an access to predict the temperature dependent BIP (k_{ij}) of PR EoS for multiple mixtures from the information of molecular structure. The advantage of PPR78 model is to allow a quick and accurate estimation of the phase equilibrium propert ies for mixtures of compounds which included in the group-interaction-parameter matrice s without the need of measurements and model-parameter regressions. The temperature-d ependent $k_{ij}(T)$ in the PPR78 model is expressed by Eq. 11.

$$k_{ij}(T) = \frac{-\frac{1}{2}E_{ij}(T) - \left(\frac{\sqrt{a_i(T)}}{b_i} - \frac{\sqrt{a_i(T)}}{b_j}\right)^2}{2\frac{\sqrt{a_i(T)a_j(T)}}{b_i b_i}} \quad (11)$$

Where T is the temperature, the a_i and b_i are component dependent parameters of PR EOS [13], and $E_{ij}(T)$ is van-Laar type function which is defined by Eq. 12 [27].

$$E_{ij}(T) = \sum_{k=1}^{Ng}\sum_{l=1}^{Ng}(\alpha_{ik} - \alpha_{jk})(\alpha_{il} - \alpha_{jl})A_{kl}\left(\frac{298.15}{T}\right)^{\frac{B_{kl}}{A_{kl}}-1} \quad [12]$$

Where N_g is the number of different groups; a_{ik} is the fraction of molecule i occupied by group k (occurrence of group k in molecule i divided by the total number of groups present in molecule i); A and B are the group-interaction parameters, $A_{kl} = A_{lk}$, $B_{kl} = B_{lk}$,, and $A_{kk} = A_{ll} = B_{kk} = B_{ll} = 0$; The subscript k and l refer to different groups.

VLE phase diagram for R32 + R1234ze(E) system was also predicted by using the PPR78 model. The most difficult point to utilize the PPR78 model is the decomposition of components R32 and R1234ze(E). R1234ze(E) could be decomposed as groups of CF_3, CH= , and =CF, but R32 is not possible to decompose by the group matrix that existed in the newest version of PPR78 model [26]. To address the issue, a new group of CH_2CF_2 was defined and added to PPR78 model in this paper by following steps: (1) to collect VLE data where R32 is involved; (2) to correlate the VLE data to the PPR78 model; and (3) to regress the group-interaction parameters.

VLE data of seven binary systems containing alkane, fluorinated alkanes, and fluorinated olefins with R32 were collected to establish a VLE database containing 1477 experimental data points. The group-interaction parameters between the new group (CH_2CF_2) and the other nine existed groups were correlated by minimizing the deviations between calculated and experimental bubble pressure from the collected VLE database. The 18 group-interaction parameters (9 A_{kl} and 9 B_{kl}) were obtained by minimizing the following objective function given by Eq. 13.

$$F_{obj.bubble} = 100 \sum_{i=1}^{n_{bubble}} \left(\left| \frac{P_{i.\exp}(T_{\exp}, x_{1.\exp}) - P_{i.cal}(T_{\exp}, x_{1.\exp})}{P_{i.\exp}(T_{\exp}, x_{1.\exp})} \right| \right) \quad (13)$$

Where n_{bubble} is the number of bubble points, $P_{\text{i,exp}}$ is the experimental bubble pressure of binary mixture at experimental temperature $T_{\text{i,exp}}$ and liquid composition $x_{\text{i,exp}}$, and $P_{\text{i,cal}}$ is the calculated bubble pressure at same experimental temperature $T_{\text{i,exp}}$ and liquid composition $x_{\text{i,exp}}$.

The data correlation was performed by a self-developed MATLAB program. Table S1 shows critical parameters of 8 pure components and Table S2 summaries the literature sources of experimental data used in this study. The correlated values for group-interaction parameters A_{kl} and B_{kl} (unit in MPa) are presented in Table 8 and 9 respectively, and the detailed correlation results are shown in Table S3 and Fig S1-S7.

For all the data points included in our database, AAD *P* and Bias *P* between calculated and experimental bubble pressure are less than 5.12% and 3.51 respectively as shown in Table S3. These results clearly indicate that the PPR78 model have a good consistent with the experimental data in our database. Fig S1-S7 illustrate the binary systems the accuracy of the proposed model.

The VLE data of R32 (1) + R1234ze(E) (2) system were predicted by PPR78 model with the group group-interaction parameters presented in Tables 8 and 9. An unexpectedly large deviation was observed in Table 10, the Bias and AAD on bubble pressure were -5.39% and 5.42% while Bias and AAD on vapor mole fractions were -1.90% and 3.86% for all of the data. The maximum AAD P is up to -8.62% at 273.14 K. Fig. 9 shows the VLE phase diagram of R32 (1) + R1234ze(E) (2) system compared with experimental data in Table 3.

The following reasons can be invoked to explain large deviation between PPR78 model and experimental data for R32 + R1234ze(E) system.

(1) The PPR78 model cannot distinguish isomers between R1234ze(E) and R1234yf. According to the decomposition principle of PPPR78 model, both R1234ze(E) and R1234yf can be decomposed into one CF_3 group, one $CH_{2,alkenic}$ /$CH_{alkenic}$ group, and one $CF_{2,double\ bond}$ or $CF_{double\ bond}$ group [26]. Therefore, although R1234yf and R1234ze(E) have different molecular structures, their group decomposition results are the same. The k_{ij} of R32+R1234yf and R32+R1234ze(E) calculated from Eq. 11 are also the same. Hence, a special attention needs to be paid when using the PPR78 model to predict the VLE of R32 + R1234ze(E), in the temperature range of 273~333 K, the PPR78 model will overestimate the equilibrium pressure, and the pressure deviation will decrease as the temperature increases.

(2) In addition, the PPR 78 model fails to predict VLE data near the critical point in correct way. For isothermal of 353 K and 363 K, the PPR78 model can only generate phase lines with mole fractions range of 0~0.7 and 0~0.5 respectively, and fails to generate the vapor-liquid coexistence data in the critical region for the mixture

Table 8. Group-interaction parameters A: ($A_{kl} = A_{lk}$)/MPa. Only the parameters in the last line of Table 8 relative to the CH_2F_2 group were determined in this work. The other parameters were determined by Qian 2017 [26].

Parameter A	CH_3 (group 1)	CH_2 (group 2)	CH (group 3)	$CH_{2,alkenic}$ /$CH_{alkenic}$ (group 3)	C_2F_6 (group 22)	CF_3 (group 23)	$CF_{2,double\ bond}$ or $CF_{double\ bond}$ (group 25)	$C_2H_4F_2$ (group 26)	$C_2H_2F_4$ (group 27)	CH_2F_2 (group 28)
CH_3 (group 1)	0	-	-	-	-	-	-	-	-	-
CH_2 (group 2)	65.54	0	-	-	-	-	-	-	-	-
CH (group 3)	214.9	39.05	0	-	-	-	-	-	-	-
$CH_{2,alkenic}$ /$CH_{alkenic}$ (group 3)	48.73	9.608	84.76	0	-	-	-	-	-	-
C_2F_6 (group 22)	119.1	105	0	124.9	0	-	-	-	-	-
CF_3 (group 23)	123.2	195.6	531.5	155.4	-14.47	0	-	-	-	-
$CF_{2,double\ bond}$ or $CF_{double\ bond}$ (group 25)	-12.29	0	0	88.21	55.9	17.55	0	-	-	-
$C_2H_4F_2$ (group 26)	128.3	107.1	143.8	76.86	0	113.2	0	0	-	-
$C_2H_2F_4$ (group 27)	158.5	86.47	121.5	64.51	60.74	28.14	0	-4.118	0	-
CH_2F_2 (group 28)	286.7	14.74	29.11	100.61	265.378	120.2	100.6	13.46	22.76	0

Table 9. Group-interaction parameters B: ($B_{kl} = B_{lk}$)/MPa. Only the parameters in the last line of Table 9 relative to the CH_2F_2 group were determined in this work. The other parameters were determined by Qian 2017 [26].

Parameter B	CH_3 (group 1)	CH_2 (group 2)	CH (group 3)	$CH_{2,alkenic}$ /$CH_{alkenic}$ (group 3)	C_2F_6 (group 22)	CF_3 (group 23)	$CF_{2,double\ bond}$ or $CF_{double\ bond}$ (group 25)	$C_2H_4F_2$ (group 26)	$C_2H_2F_4$ (group 27)	CH_2F_2 (group 28)
CH_3 (group 1)	0	-	-	-	-	-	-	-	-	-
CH_2 (group 2)	105.7	0	-	-	-	-	-	-	-	-
CH (group 3)	294.9	41.59	0	-	-	-	-	-	-	-
$CH_{2,alkenic}$ /$CH_{alkenic}$ (group 3)	44.27	50.79	193.2	0	-	-	-	-	-	-
C_2F_6 (group 22)	118.4	130.4	0	219.6	0	-	-	-	-	-
CF_3 (group 23)	133.8	199	-1945	154.4	-87.05	0	-	-	-	-
$CF_{2,double\ bond}$ or $CF_{double\ bond}$ (group 25)	16.54	0	0	12.87	-193.3	-92.99	0	-	-	-
$C_2H_4F_2$ (group 26)	292.4	119.8	15.78	-145.5	0	247.1	0	0	-	-
$C_2H_2F_4$ (group 27)	356.5	-40.49	-44.61	-41.86	217.6	8.235	0	4.118	0	-
CH_2F_2 (group 28)	369.0	115.8	72.17	116.0	42.59	176.2	116.0	112.2	115.0	0

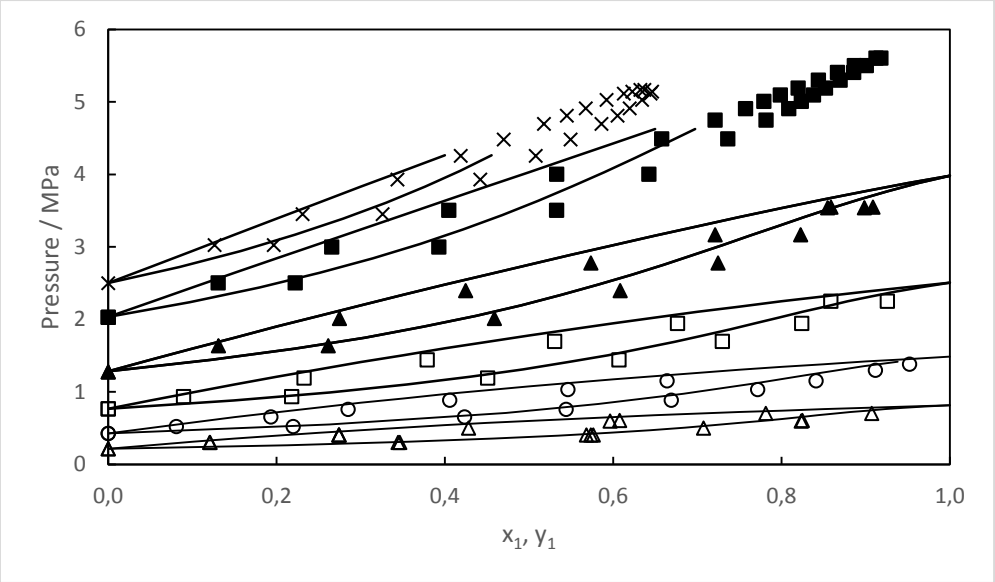

Figure 9: P-x-y diagram of the R32 (1) - R1234ze(E) (2) system. Experimental data: (Δ) 273.14 K; (○) 293.17 K; (□) 313.20 K; (▲) 333.27 K; (■): 353.53 K; (×) 363.32 K; solid line: PPR78 model.

Table 10: AAD and Bias on bubble pressure and vapor mole fractions: comparison between PPR78 model calculations and experimental data of this work.

T/*K*	Bias *P*/%	AAD *P*/%	Bias y_1/%	AAD y_1/%
273.14	-8.62	8.70	-6.00	6.34
293.17	-6.16	6.22	-3.95	5.00
313.2	-5.26	5.26	-1.99	2.99
333.27	-4.32	4.32	-0.04	1.51
353.53	-3.04	3.04	2.14	2.51
363.32	-1.45	1.45	3.29	3.29
all data	-5.39	5.42	-1.90	3.86

5. Conclusion

In this paper, VLE data at seven temperatures for the R32 + R1234ze(E) system are presented. They were obtained using an experimental technique based on a "static-analytic" method. The data were correlated by the Peng Robinson EoS, with the original alpha function and the Wong-Sandler mixing rules involving the NRTL model. Moreover, REFPROP 10.0 with the existing model was used to correlate our data and the data from literature. It was found that the two models give results in very good agreement with experiments. We have also extended PPR78 model to R32-containing

systems. The new R32 group was defined, and the missing parameters in the PPR78 model were fitted using both literature data and data provided in this work. The phase equilibrium of the mixture was predicted by PPR78 model with the new group parameters, and the shortcomings of the existing PPR78 model, particularly for temperature above critical temperature of R32, were found through comparison with experimental data. We can notice that (1) REFPROP model parameters should be revised to include the new set of experimental data presented in this work; (2) The existing group decomposition principles of PPR78 model should be improved in the VLE calculation for HFOs-containing systems. Addition of subgroups should be considered for $CF_{2,\text{double bond}}$ or $CF_{\text{double bond}}$ group.

List of symbols:

a	Parameter of the equation of state (energy parameter [J. m^3.mol^{-2}])
b	Parameter of the equation of state (molar co volume parameter [m^3.mol^{-1}])
C	Numerical constant equal to -0.62323
F	Objective function
g	Molar Gibbs energy [J. mol^{-1}]
k_{ij}	Binary interaction parameter
P	Pressure [MPa]
R	Gas constant [J.mol^{-1}.K^{-1}]
T	Temperature [K]
U	Liquid or vapor mole fractions
x	Liquid mole fraction
y	Vapor mole fraction

Greek letters:

α_{ij}	non randomness NRTL model parameter (Eq. 5)
α_{12}	Relative volatility
τ_{ij}	NRTL model binary interaction parameter (Eq. 5), [J. mol^{-1}]
β	constant used in the Eq. 9
λ_i	parameters used in the Eqs. 9 and 10
ρ	Density
σ_{ij}	Diameter
ω	Acentric factor
ΔU	Deviation (U_{exp}-U_{cal})

Superscript

Chain	Chain contribution interaction
Disp	Dispersion contribution interaction
hc	Hard chain
hs	Hard sphere
E	Excess property
0	Initial state

Subscripts

C	Critical property
cal	Calculated property
exp	Experimental property
i,j	Molecular species
1	R32
2	R1234ze(E)

Abbreviation

GWP	Global Warming Potential
PR EoS	Peng-Robinson Equation of State
VLE	Vapour-Liquid Equilibrium

References:

[1] I. Sarbu, A review on substitution strategy of non-ecological refrigerants from vapour compression-based refrigeration, air-conditioning and heat pump systems, Int. J. Refrig. 46 (2016) 123-141

[2] UNEP, The Kigali Amendment to the Montreal Protocol: HFC Phase-down.OzonAction Fact Sheet, in, 2016.

[3] N. V., HFO refrigerants: A review of present status and future prospects, Int. J. Refrig, 122 (2021) 156-170.

[4] A. Mota-Babiloni, J. Navarro-Esbrí, F. Molés, Á.B. Cervera, B. Peris, G. Verdú, A review of refrigerant R1234ze(E) recent investigations, Appl. Therm. Eng. 95 (2016) 211-222.

[5] S. Bobbo, C. Zilio, M. Scattolini, L. Fedele, R1234yf as a substitute of R134a in automotive air conditioning. Solubility measurements in two commercial PAG oils., Int. J. Refrig., 40 (2014) 302–308.

[6] Y. Liu, A. Valtz, J. El Abbadi, G. He, C. Coquelet, Isothermal Vapor–Liquid Equilibrium Measurements for the (R1234ze(E) + Ethane) System at Temperatures from 272.27 to 347.52 K., J Chem Eng Data, 63 (2018) 4185–4192.

[7] Z. Yang, A. Valtz, C. Coquelet, J. Wu, J. Lu, Experimental measurement and modelling of vapor-liquid equilibrium for 3,3,3- Trifluoropropene (R1243zf) and trans-1,3,3,3-Tetrafluoropropene (R1234ze(E)) binary system, Int. J. Refrig. , 120 (2020) 137–149.

[8] S. Wang, R. Fauve, C. Coquelet, A. Valtz, C. Houriez, P.A. Artola, E.E. Ahmar, B. Rousseau, H. Hu, Vapor-liquid equilibrium and molecular simulation data for carbon dioxide (CO2) + trans-1,3,3,3-tetrafluoroprop-1-ene (R-1234ze(E)) mixture at temperatures from 283.32 to 353.02 K and pressures up to 7.6 MPa, Int J. of Refrig. 98 (2019) 362-371.

[9] I. Sarbu, A review on substitution strategy of non-ecological refrigerants from vapour compression-based refrigeration, air-conditioning and heat pump systems, Int. J. Refrig. 46 (2014) 123-141.

[10] X. Hu, X. Meng, J. Wu, Isothermal vapor liquid equilibrium measurements for difluoromethane (R32) + trans-1,3,3,3-tetrafluoropropene (R1234ze(E)), Fluid Ph. Equilib. 431 (2017) 58-65.

[11] R. Akasaka, Thermodynamic property models for the difluoromethane (R-32)+trans-1,3,3,3-tetrafluoropropene (R-1234ze(E)) and difluoromethane+2,3,3,3-tetrafluoropropene (R-1234yf) mixtures, Fluid Ph. Equilib. 358 (2013) 98–104.

[12] E.W. Lemmon, I.H. Bell, M.L. Huber, M.O. McLinden, NIST Reference Fluid Thermodynamic and Transport Properties Database (REFPROP), Version 10.0; Standard Reference Data, in, National Institute of Standards and Technology: Gaithersburg, MD, 2018.

[13] D.Y. Peng, D.B. Robinson, A new two-constant equation of state, Ind. Eng.Chem. Fundam, 15 (1976) 59-64.

[14] D.S.H. Wong, S.I. Sandler, A theoretically correct mixing rule for cubic equations of state, AIChE Journal, 38 (1992) 671–680.

[15] H. Renon, J.M. Prausnitz, Local Compositions in Thermodynamic Excess Functions for Liquid Mixtures, AICHE Journal, 14 (1968) 135–143.

[16] J.-N.l. Jaubert, R. Privat, F. Mutelet, Predicting the Phase Equilibria of Synthetic Petroleum Fluids with the PPR78 Approach, AIChE J, 56 (2010) 3225–3235.
[17] C. Coquelet, A. Valtz, P. Théveneau, Experimental Determination of Thermophysical Properties of Working Fluids for ORC Applications, in: ORC for Waste Heat Recovery Applications, IntechOpen, 2019.
[18] W. Afzal, A. Valtz, C. Coquelet, Vapour-liquid equilibria of ethane and ethyl mercaptan: experiments and modelling, J. Nat. Gas Eng. 3 (2019) 96-108.
[19] D. Richon, Procédé et dispositif pour prélever des micro-échantillons d'un fluide sous pression contenu dans un container, FR-A-2 853, Armines's Patent, 2004, France.
[20] E. Åberg, A. Gustavsson, Design and evaluation of modified simplex methods, Anal. Chim. acta, 144 (1982) 39-53.
[21] P. Ungerer, B. Tavitian, A. Boutin, Application of Molecular Simulation in The Oil and Gaz Industry – Monte Carlo Methods, Edition Technip ed., Paris, 2005.
[22] R. Stockfleth, R. Dohrn, An algorithm for calculating critical points in multicomponent mixtures which can easily be implemented in existing programs to calculate phase equilibria, Fluid Ph. Equilib. 145 (1998) 43-52.
[23] R.A. Heidemann, A.M. Khalil, The calculation of critical points,. AIChE J. , 26 (1980) 769 - 779
[24] M.L. Michelsen, R.A. Heidemann, Calculation of critical points from cubic two-constant equations of state, AIChE J., 27 (1981) 521 – 523
[25] J.-N.e. Jaubert, F. Mutelet, VLE predictions with the Peng–Robinson equation of state and temperature dependent kij calculated through a group contribution method, Fluid Ph. Equilib. 224 (2004) 285–304.
[26] J.-W. Qian, R. Privat, C. Coquelet, J.-N. Jaubert, D. Ramjugernath, Fluid-phase-equilibrium prediction of fluorocompound-containing binary systems with the predictive E-PPR78 model, Int. J. Refrig. 73 (2017) 65–90.
[27] J.-N. Jaubert, J. Qian, R. Privat, C.F. Leibovici Reliability of the correlation allowing the kij to switch from an alpha function to another one in hydrogen-containing systems, Fluid Ph. Equilib. 338 (2013) 23– 29.